SCIENTIFIC REPORTS

Correspondence and
requests for materials
should be addressed to
L.X. (linxu@jlu.edu.cn)
or D.L. (ldl@jlu.edu.cn)

Synthesis of Au/Graphene Oxide Composites for Selective and Sensitive Electrochemical Detection of Ascorbic Acid

Jian Song, Lin Xu, Ruiqing Xing, Qingling Li, Chunyang Zhou, Dali Liu & Hongwei Song

State Key Laboratory on Integrated Optoelectronics, College of Electronic Science and Engineering, Jilin University, 2699 Qianjin Street, Changchun, 130012, People's Republic of China.

In this work, we present a novel ascorbic acid (AA) sensor applied to the detection of AA in human sera and pharmaceuticals. A series of Au nanoparticles (NPs) and graphene oxide sheets (Au NP/GO) composites were successfully synthesized by reduction of gold (III) using sodium citrate. Then the Au NP/GO composites were used to construct nonenzymatic electrodes in practical AA measurement. The electrode that has the best performance presents attractive analytical features, such as a low working potential of $+0.15$ V, a high sensitivity of 101.86 μA mM^{-1} cm^{-2} to AA, a low detection limit of 100 nM, good reproducibility and excellent selectivity. And more,it was also employed to accurately and practically detect AA in human serum and clinical vitamin C tablet with the existence of some food additive. The enhanced AA electrochemical properties of the Au NP/GO modified electrode in our work can be attributed to the improvement of electroactive surface area of Au NPs and the synergistic effect from the combination of Au NPs and GO sheets. This work shows that the Au NP/GO/GCEs hold the prospect for sensitive and selective determination of AA in practical clinical application.

Ascorbic acid (AA), commonly called vitamin C, is one of the most important nutrients and effective antioxidant in protecting human from oxidative stress[1–3]. Today, AA is widely used in biomedical chemistry, diagnostics and the identification of food ingredients. The concentration of AA is usually kept in a low level, so accurate detection of AA content is of great importance to guarantee health conditions and food security[4,5]. However, some other accompanied electroactive compounds of similar electrochemical properties with AA, such as dopamine (DA) and uric acid (UA) glucose, and other oxidizable species, complicate their electrochemical identification, especially in biological environment[6,7]. Hence, the clear separation of the electrochemical signals of AA from these compounds is still a great challenge.

In the past few decades, electrochemical techniques have been used to detect small biomolecules owing to their high sensitivity, rapid response, flexibility, and low expense[8,9]. In an electrochemical system, the AA voltammetric peak can be separated from that of interfering species using functional material modified electrodes[10,11]. Compounding two different reasonable selected materials is an effective way to further improve the electrochemical properties[12–14]. Specifically, GO sheets have been considered as a suitable substrate for assembling nanomaterials because of their large surface area, excellent thermal and mechanical properties and chemical modification capability. In addition, they exhibit specific properties such as hydrophilicity, multiple oxygen moieties, and controllable electronic properties[15–18]. Meanwhile, in recent years, Au NPs have been widely investigated and applied to molecular catalysis, biosensors, and mutifunctional reagents due to their quantum size effect[19–21]. Therefore, there is a potential development of a non-enzymatic electrochemical biosensor for AA involving the complementary use of GO sheets and Au NPs. For example, Tian *et al.* used a Au NP-β-cyclodextrin-graphene modified electrode to detect AA, DA and UA[22]. The detection limit for AA (based on S/N = 3) is 10 μM and the linear response range is 30–2000 μM. Zhang et al. used a facile one-step method to fabricate nanoflower-like dendritic Au NPs and polyaniline composite nanosheets and applied them on glass carbon electrode as an AA sensor[14]. A linear relation between the current response and the AA concentration was obtained between 10 μM and 12 mM, with a detection limit of 8.3 μM (S/N = 3) and the sensitivity of 25.69 μA mM^{-1} cm^{-2}. However,

1

there have been very few reports on the detection of AA in real-life human sera or pharmaceuticals to demonstrate the practical applications of AA biosensors.

In this work, we have chemically reduced Au(III) using sodium citrate to form Au NPs of approximately 13–16 nm average diameter on GO sheets[23]. These Au NP/GO composite nanomaterials were then immobilized on the glass carbon electrodes (GCE) for AA detection. These modified electrodes were used to monitor AA concentration in real-life human sera and pharmaceuticals.

Results and Discussion

Characterization of the Au NP/GO composites. The morphology of the GO sheets used in this work was first examined by transmission electron microscope (TEM) technique, and the results are shown in Fig. 1a. The GO sheets exhibit flake-like shape and is few-layer flexible wrinkled. The smooth and planar surface indicates that GO sheets can provide a high surface to volume ratio and a 2D structure, which is necessary for loading Au NPs. Then the GO sheets were surface loaded with different amount of Au NPs (Fig. 1b–1e). As can be seen, the loaded Au demonstrates regular small NP morphology and can grow on the GO sheet independently. The size histograms of Au NPs in each sample were carefully measured and shown in Fig. S2. The size distribution of Au NPs shows a slightly growing trend from S_1 to S_4 and the average size of S_1, S_2, S_3 and S_4 are determined to be 13.3, 14.2, 15.3 and 16.0 nm, respectively. Besides, as the amount of initial $HAuCl_4$ gradually increased, the amount of Au NPs loaded on the GO sheets also increased. Note that when the amount of initial $HAuCl_4$ reached

20 mg, the Au NPs loaded on the GO sheet tended to aggregate together (Fig. 1e). Fig. 1f shows the high resolution TEM (HRTEM) image, in which the interplanar distances can be clearly seen. The as marked interplanar distances are 0.235 nm and 0.202 nm, corresponding to the (111) and (200) face of face-centered cubic Au, respectively. The inset of Fig. 1f is the selected area electron diffraction (SAED) pattern of Au NP/GO composites (S_3). The diffraction patterns irregularly distribute and the diffraction rings can be observed, which indicates this sample yields a polycrystalline structure[24]. The conditions of the other samples are the same.

The Energy-dispersive X-ray spectra (EDX) were measured to characterize the elemental heterogeneity of Au NP/GO composites (S_1, S_2, S_3 and S_4), as shown in Fig. S1 (see in supporting information). The representation of Au, C and O elements further indicates the existence of GO and Au. The strong Cu and Si peaks are attributed to the substrates. The crystal structure of Au NP/GO composites (S_1, S_2, S_3 and S_4) was characterized by X-ray diffraction (XRD) patterns, and the results obtained are shown in Fig. 2a. All the four Au NP/GO composites show similar XRD peaks, which well match to the face-centered cubic crystalline Au (JCPDS 04-0784) and no any trace of other phases is detected. This indicate that the increasing concentration of $HAuCl_4$ bring no influence to the crystal structure. Since the GO powder does not have a crystal structure, no obvious characteristic peak of GO can be distinguished.

The Raman spectra of Au NP/GO composites compared with pure GO are shown in Fig. 2b. In the studied range, all the samples have two similar characteristic Raman peaks, which belong to the D and G
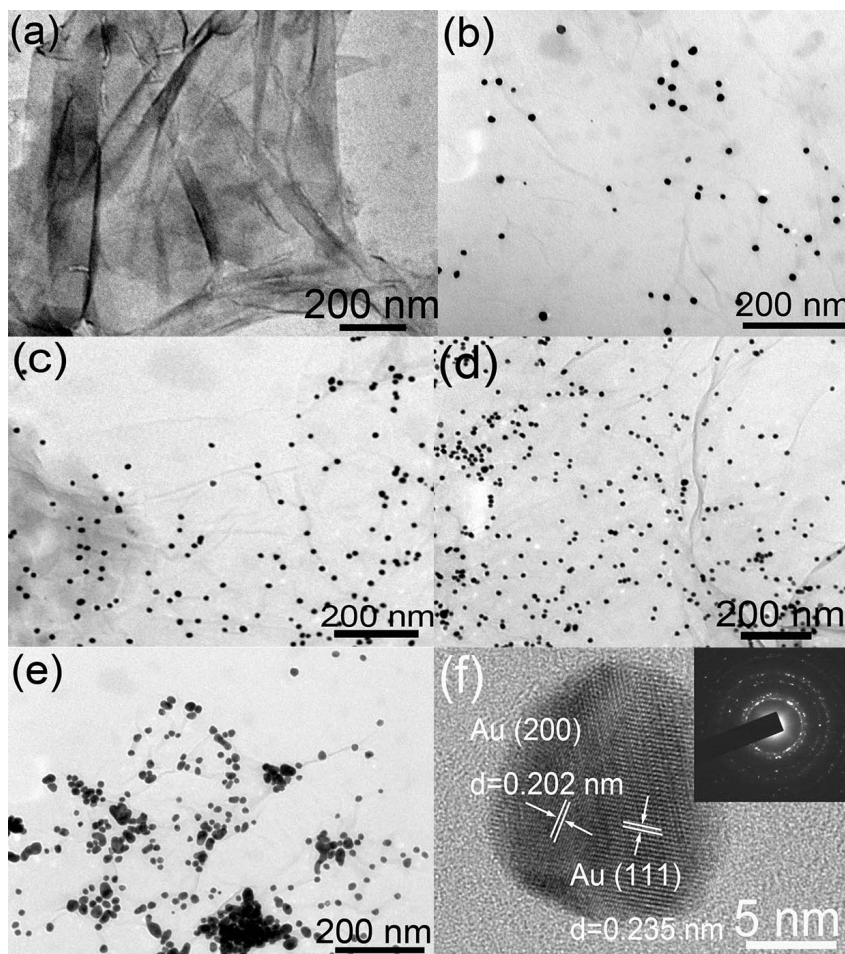

Figure 1 | TEM images of (a) GO sheets. (b–e) Au NP/GO composites based on S_1, S_2, S_3 and S_4. (f) HRTEM image of Au/GO composite based on S_3, the inset is the corresponding SEAD pattern.
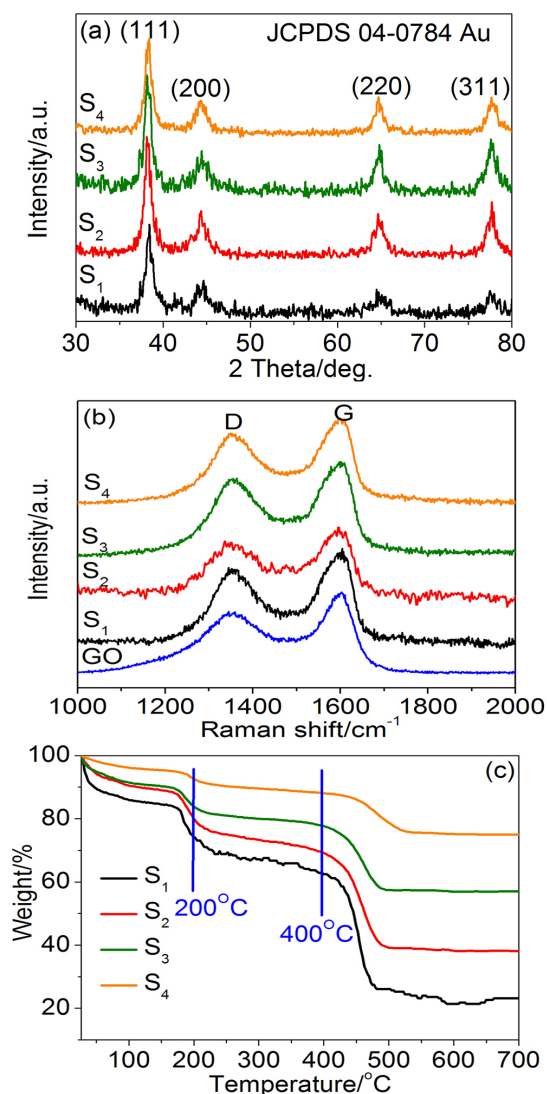
Figure 2 | (a) XRD patterns of Au/GO composites S_1, S_2, S_3 and S_4. (b) Raman spectra of GO and Au/GO composites. (c) TGA curves of S_1, S_2, S_3 and S_4 samples.

bands of GO sheets. The disorder-induced D bands at 1351 cm^{-1} arising from sp^3-hybridized carbon were observed[25]. The tangential stretch G band represents the E_{2g} zone center mode of the crystalline graphite. Generally, the relative intensity ratio of the D and G bands (I_D/I_G) depends strongly on the degree of disorder in the graphitic material[26]. Generally, the I_D/I_G ratio increases when more defects are brought into GO. According to Fig. 2b, the I_D/I_G ratios of the four Au NP/GO composites are calculated to be 0.80, 0.82, 0.81 and 0.82, respectively, which are a little higher than that of pure GO sheet (0.77). This shows that the loading amount of Au NPs has only a little influence on the I_D/I_G ratio, implying that the nucleation of Au NPs at GO surfaces introduces very few defects into the GO structure.

To further confirm the concentration of Au and GO in each composite sample, thermogravimetric analysis (TGA) curves were investigated. As shown in Fig. 2c, the mass loss below 200°C (25.7%, 19.8%, 16.2% and 8.2% for S_1, S_2, S_3, and S_4, respectively) can be attributed to the evaporation of adsorbed water. The slight mass loss between 200°C and 400°C (12.4%, 10.3%, 6.0% and 4.4% for S_1, S_2, S_3, and S_4, respectively) arose from the decomposition of some residual oxygen-containing groups[27]. Then the finial significant mass loss occurred when the Au NP/GO composites were heated above 400°C

(38.6%, 30.8%, 20.5 and 12.9% for S_1, S_2, S_3, and S_4, respectively). This was most likely caused by the decomposition of carbon skeleton from GO[27]. Accordingly, the mass percentage of Au in S_1, S_2, S_3 and S_4 are calculated to be 24.0%, 39.0%, 57.4% and 75.5%, respectively, which also implies the successful loading of Au NPs on GO sheets.

Enhanced electrochemistry behavior of Au NP/GO/GCEs toward AA detection. To determine the working condition of effective detecting AA, the Au/GO/GCEs were first characterized by cyclic voltammetry (CVs) between the potentials of −0.4 and +0.6 V in 0.1 M phosphate-buffered solution (PBS) at a scan rate of 100 mV/s. First the CVs in the absence (shown in black trace) and presence (shown in green trace) of 1 mM AA of different electrodes were measured and shown in Fig. 3a. To compare, the CV curves at a bare electrode and a GO/GCE was conducted and the results obtained are shown in Fig. S3 (supporting information). As can be observed, the position of oxidation peak of AA for bare electrode is about +0.3 V, corresponding to the irreversible oxidation of AA (see Fig. S3a). After surface modified by pure GO sheets (Fig. S3b), no clear response current change can be found after addition of AA. The reason can be summarized as the electrical conductivity of GO is not as good as that of graphene and other metal materials which contain much free electrons. However, after loading Au NPs on GO sheets (take S_3 for example, Fig. 3a), a broad and clear oxidation peak with a peak potential of about +0.15 V was observed again after the addition of 1 mM AA and the potential value was one time lower than that of bare GCE. The appearance and shift of the oxidation peak in Au NP/GO/GCE can be attributed to the synergistic effects between Au NPs and GO sheets. Since the interfering substances like UA, DA, and NADH are always coexisted with AA and the oxidation peak position of them are usually around +0.2 V to +0.5 V[6,22,28]. The decrease of the peak position of Au/GO/GCE (from +0.3 V to +0.15 V) is important for avoiding the influence. Particularly, the oxidation peak might correspond to the oxidation reaction of AA occurring on the electrode surface. The electro-oxidation mechanism of AA is illustrated in Fig. 3c. The AA molecules in the solution were adsorbed onto the surface of Au NP/GO/GCE. Then the AA molecules hydrolyzed with water were oxidized to dehydroascorbic acid[29]. The oxidation process of AA can release electrons and the current can be detected at a constant working voltage.

In addition, the Au NP/GO/GCEs based on different samples (S_1, S_2, S_3, and S_4) were further investigated and compared, which can give more information about the difference of the electron transfer kinetics on the electrode surface. As shown in Fig. 3b, all the Au/GO/GCEs appear similar broad reduction peak round +0.15 V. With increasing of loading amount of Au NPs, the corresponding peak currents of the Au NP/GO/GCEs also show a rising trend at first and reach the maximum value at Au NP/GO/GCE based on S_3. After that, when further increasing the loading amount of Au NPs (S_4) the peak current shows a decreased trend, the reason can be ascribed to the aggregation of Au NPs on GO sheets as shown in Fig. 1d, which may cause the decline of surface area. The peak current values of Au NP/GO/GCEs based on S_1, S_2, S_3 and S_4 samples were measured to be 2.4, 3.6, 5.5 and 4.2 μA, respectively. That is to say, Au/GO/GCE based on S_3 exhibits the best performance for AA detection, which can be attributed to the enough loading amount and well dispersion of Au NPs on GO sheets.

The electrochemical controlled process is further studied through the CVs of 0.1 M PBS solution at a S_3 Au NP/GO/GCE at different scan rates after injection of 1 mM AA, as depicted in Fig. S4. The redox peak currents increase linearly with the scan rate in the range of 50–250 mV/s, indicating a surface-controlled electrochemical process[30].

Amperometric detection of AA of Au NP/GO/GCEs. To determine the amperometric sensing application of Au/GO/GCEs, current-time (I-t) curves were performed at +0.15 V (vs. Ag/AgCl) in
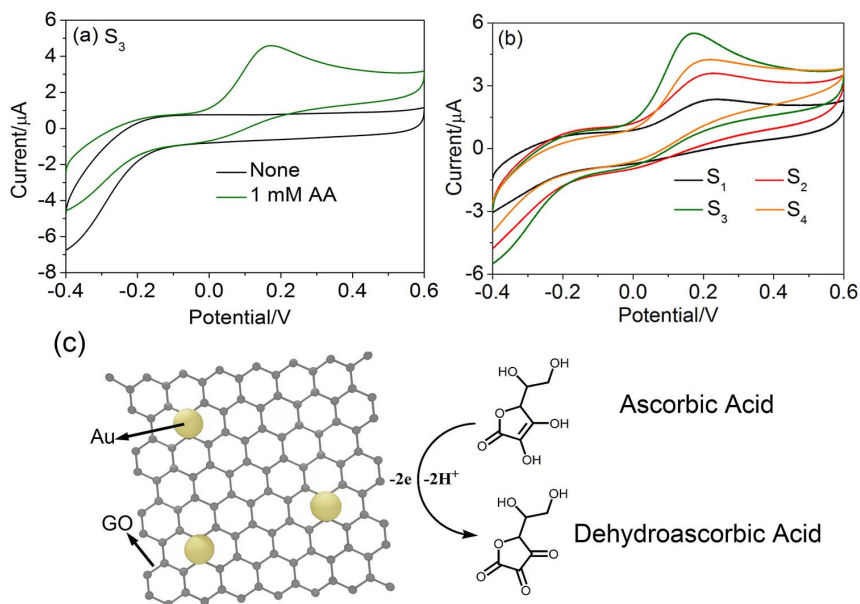
Figure 3 | CV curves of (a) Au/GO composite (S_3) in 0.1 M PBS solution with the absence (black trace) and presence (green trace) of 1 mM AA. (b) Au/GO composites (S_1, S_2, S_3 and S_4) in 0.1 M PBS solution with the present of 1 mM AA. (c) Schematic illustration of AA sensing mechanism by using Au/GO composite.

0.1 M PBS solution. Fig. 4a shows the typical amperometric responses of S_1, S_2, S_3 and S_4 by successive addition of certain amount of AA. Well-defined, stable and fast amperometric response could be observed. Similar with the CVs behavior, the Au NP/GO/GCE based on S_3 shows the best sensitive response with the change of AA concentration. The calibration curves corresponding to four Au/GO/GCEs are shown in Fig. 4b, and all these electrodes display good linearity. According to the calibration curves, the sensitivity, linearity range and response time of each electrodes were calculated and listed in Table 1. The linear regression

equations were carefully calculated and shown in Table 2. As is listed, with the increasing amount of loaded Au NPs on GO sheets (from S_1 to S_3), the corresponding sensitivity gradually increases and the detection limit gradually reduces. The Au NP/GO/GCE based on S_4 tend to decrease on sensitivity since the Au NPs on the GO sheets started to aggregate together. The response times of Au/GO/GCEs based on S_1, S_2, S_3 and S_4 are determined after injected in 100 μM AA, respectively. As can be clearly seen in Table 1, the increasing amount of Au NPs can significantly improve the response speed. Fig. 4c shows the obvious amperometric response of Au NP/GO/
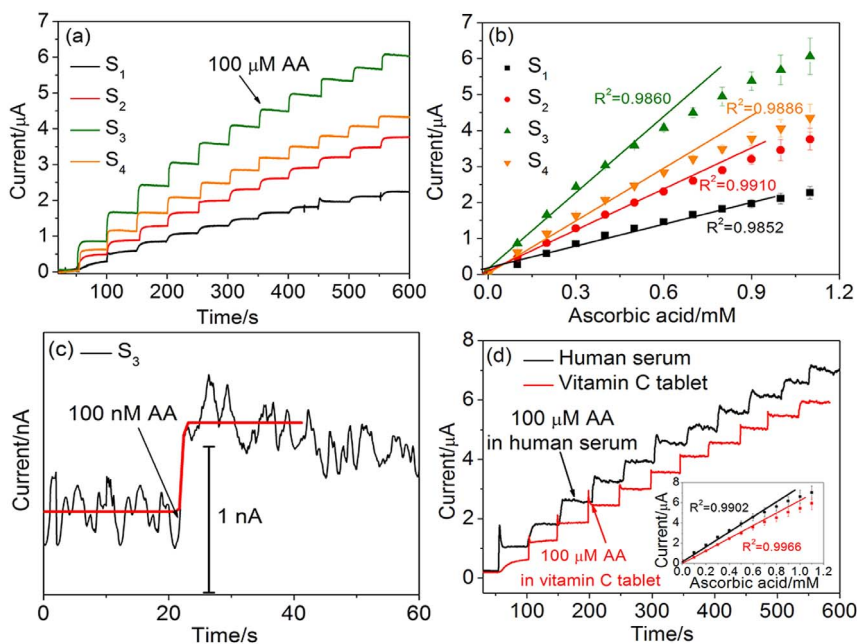

Figure 4 | Amperometric response of (a) S_1, S_2, S_3 and S_4 to successive additions of 0.1 mM AA at an applied potential of 0.15 V. (b) The corresponding calibration curves of (a). (c) S_3 to the additions of 100 nM AA at an applied potential of +0.15 V. (d) S_3 to successive additions of human serum (black trace) and Vitamin C tablet (red trace) contained 100 μM AA. Inset is the corresponding calibration curves of (d).

Table 1 | A list of AA sensing properties of different electrodes at an applied potential of 0.15 V

Sample	Sensitivity/$\mu A\ mM^{-1}\ cm^{-2}$	R^2	Linear range	Response time/s
S_1	29.05	0.9852	1.21 μM to 1 mM	12.5
S_2	53.39	0.9910	0.86 μM to 0.8 mM	7.1
S_3	101.86	0.9860	0.11 μM to 0.6 mM	4.2
S_4	68.53	0.9886	0.39 μM to 0.7 mM	4.6

GCE based on S_3 after the addition of 100 nM AA with a signal-to-noise ratio (S/N) of ~3 in order to obtain the accurate detection limit. This result is much lower than the previously reported graphene-based electrochemical sensors and electrical sensors assisted by enzymes as listed in Table 3. Besides, as compared, the Au NP/GO/GCE based on S_3 in this work also shows high sensitivity, low detection limit and large liner range. According to the sensitivity improvement, two factors need to be considered: On the one hand, the amount of Au NPs influences dominantly on the performance when they are gradually increased. The reason can be attributed to the good electrical conductivity and large surface area introduced by Au NPs. The Au NPs on S_4 tend to aggregate together so the surface area decreases and the sensitivity is negatively influenced. On the other hand, the GO sheets can provide a large area for the Au NPs loading, so they can grow independently without aggregating in a certain amount range. So the GO sheets also make a great contribution to the improvement of the sensitivity.

Moreover, the practical AA sensing ability of Au NP/GO/GCE based on S_3 was further investigated in real human serum with Au NP/GO/GCE based on S_3 and in clinical vitamin C tablet. As shown in Fig. 4d, the I–t curve corresponds to human serum was obtained by adding human serum contained 100 μM AA, and the I–t curve corresponds to vitamin C tablet was gotten by addition of aqueous solution of vitamin C tablet which contained 100 μM AA. As can be seen, the amperometric response of the vitamin C tablet is slightly lower than that in human serum. It may caused by the food additives in vitamin C tablet which may attach on and then fouling the electrode surface. The inset of Fig. 4d shows the calibration curves and both of them display good linearity in the range of 0.1–0.6 mM. The sensitivities of the Au NP/GO/GCE based on S_3 are calculated to be 108.82 $\mu AmM^{-1}cm^{-2}$ and 89.76 $\mu AmM^{-1}cm^{-2}$ corresponding to the human serum and vitamin C tablet environments. The error ranges are 106.87% and 88.12% for the human serum and vitamin C tablet environments after calculated.

Reproducibility, stability, anti-interference property of the Au NP/GO/GCEs. The reproducibility, stability and anti-interference property of Au NP/GO/GCE based on S_3 were further evaluated. For reproducibility, five same Au NP/GO/GCEs based on S_3 were investigated at +0.15 V to compare their amperometric current responses. The relative standard deviation (R.S.D.) was 8.4%, confirming that the preparation method was highly reproducible. The stability of Au NP/GO/GCE based on S_3 was tested once per week in 0.1 M PBS solution at a scan rate of 100 mV/s and lasted for a month (data not shown). The sensitivity decrease of the electrode was no more than 10%, indicating a good stability of Au NP/GO/GCE. Since there are many interfering substances coexist with AA in the reported normal physiological concentration, the selectivity will be a big restrictive factor for the measurement[34–37]. Here, anti-interference property were carried out by successive injection of 100 μM AA, UA, NADH, glucose and 10 μM DA depending on the normal physiological concentration, which are the most common coexistence material of AA. The normal physiological concentration for DA is about 100 nM[34], which is 100 times lower than the concentration we injected. The CV curves obtained by detecting UA, DA and NADH independently or simultaneously were first shown in Fig. S5 in supporting information. As seen in Fig. S5a, the oxidation peak positions of UA, DA, and NADH are +0.3 V, +0.4 V, and +0.55 V, respectively, which are much higher than that of AA (+0.15 V). When the 1 mM UA, 0.1 mM DA, and 1 mM NADH coexist with 1 mM AA, the CV curve shows an obvious oxidation peak at +0.15 V, corresponding to oxide peak of AA. This indicates that the other interfering substances have a little influence on that of AA. In order to further prove the fact, amperometric response of S_3 modified electrode at +0.15 V with successive additions of different analytes are shown in Fig. 5, and the current responses of interfering species are also calculated accurately. Compared to AA, the current responses of interfering species are determined to be 4.7% (100 μM UA), 3.5% (100 μM NADH) and 8.2% (10 μM DA) at +0.15 V. It can be concluded that similar amount of these interfering substances can be neglected. The excellent sensitivity indicates the potential practical application of the as-prepared AA sensor.

Conclusions

In conclusion, we have successfully synthesized a series of Au NP/GO composites. The loading amount of Au NPs on GO sheets control of Au NP/GO composite has been investigated and the as–prepared samples are used to detect AA. The optimal sample of these Au NP/GO composites sheets is S_3 which presents high sensitivity and low detection limit compared to the other samples. The sensor also shows good reproducibility, excellent selectivity and accurate measurement in real serum sample and vitamin C tablet. The reason can be attributed to the improvement of electroactive surface area of Au NPs on GO sheets and the synergistic effect from the combination of Au NPs and GO. It is anticipated that the Au NP/GO composite material holds great potential for developing novel AA sensors.

Methods

Materials. All chemicals used were analytical grade and without further purification. GO sheets were purchased from Nanjing XFNANO Materials Tech Co., Ltd. KH_2PO_4 (99.5%), KCl (99%), Na_2HPO_4 (99%), NaCl (99.5%) and sodium citrate ($C_6H_5Na_3O_7\cdot2H_2O$, 99%) were purchased from Beijing Chemical Works. $HAuCl_4\cdot3H_2O$ (99.9%), Chitosan (93%), AA (99%), DA (99%), UA (99%) and NADH (97%) were supplied by Sigma-Aldrich. PBS (0.1 M, pH 7.4) was prepared by dispersing 0.2 g KCl, 8 g NaCl, 0.2 g KH_2PO_4 and 1.54 g Na_2HPO_4 in 1 L deionized water.

Table 2 | Particle size, Au to carbon ratio and linear regression equations for S_1, S_2, S_3 and S_4

	Particle Size/nm	Concentration of Au	Linear Regression Equations
S_1	13.3	24.0%	I (μA) = 2.03431c (mM) + 0.16937
S_2	14.2	39.0%	I (μA) = 3.73879c (mM) + 0.13651
S_3	15.8	57.4%	I (μA) = 7.13305c (mM) + 0.11692
S_4	16.0	75.5%	I (μA) = 4.79901c (mM) + 0.09919

Table 3 | Comparison of the Au/GO/GCEs with other AA sensors

Electrodes	Working potential/V	Sensitivity/$\mu A\ mM^{-1}\ cm^{-2}$	Detection limit/μM	Ref.
Au/GO/GCE	0.15	101.86	0.11	This work
SiW$_{12}$-CNTs-PAn	0.4	22.11(0–10 μM) 266.5(0.01–9 mM)	0.51	31
Au-PANI	0.2	25.69	8.2	14
P-APTT	0.255	140.8 ± 14.08	0.14	32
EMGON5-1	0.38	78.63	1.54	33
3DGF/CuO nanoflowers	0.2	2060	0.43	7
IrO$_x$ nanofibers	−0.01	194.4 ± 6.8	0.4	10

Preparation of Au NP/GO composite. To synthesize Au NP/GO composites, 4 mg GO was dispersed in 50 mL deionized water under magnetic stirring at room temperature for 1 h, before 5, 10, 15 and 20 mg HAuCl$_4$ was added, respectively. These corresponding composite suspensions were then labeled as S$_1$, S$_2$, S$_3$ and S$_4$. The composite suspensions were left for 30 min to promote the interaction of gold ions with the graphene surface. Next, 5 mL sodium citrate solution (with a sodium citrate to deionized water mass ratio of 0.02) was added under magnetic stirring for 30 min. Then the solution was heated to 80°C and kept for 1 h. Finally, the nanocomposites were obtained by washing the corresponding solution for 3 times with distilled water and by centrifugating (7000 rpm) to remove the free Au NPs formed in solution. The final Au NP/GO modified composites were collected after placed in a 60°C oven for 12 h. Moreover, the Au NP/GO was synthesized in 100°C for comparison and examined by TEM technique shown in Fig. S6.

Preparation of Au NP/GO modified electrodes. Before surface modification, a GCE (dia. 3 mm) was polished with 1 μm and 0.05 μm alumina slurries sequentially, and was rinsed with deionized water. Finally, the electrode was sonicated in nitric acid (0.2 M), acetone, ethanol, and deionized water, respectively. Then the GCE was placed in 0.5 M H$_2$SO$_4$ and 100 cyclic voltammetry scans were conducted between −1.0 and +1.0 V to introduce some active functional groups (e.g. hydroxy and carboxyl) on the electrode surface[22]. This GCE was then washed and dried at room temperature and was ready for modification. In the solution used for electrode modification, a mixture of 5 mg Au NP/GO and 1 mL ethanol was sonicated for 1 h. Then 5 μL different suspensions were applied to the GCE, respectively. After that, 5 μL of 0.2 wt% chitosan solution was applied to the electrode surface to immobilize the Au NP/GO. The as-prepared electrodes (denote as Au NP/GO/GCE) were air-dried at room temperature before usage.

Apparatus. The TEM and HRTEM images of the samples were inspected using JEM-2010 (JEOL, Japan) under a working voltage of 200 kV. XRD patterns were conducted on a Rigaku D/max 2550 X-ray diffractometer, using a mono-chromatized Cu target radiation source (λ = 1.54 Å) (Japan). TGA data were acquired on a SDT 2960 differential thermal analyzer (TA Instruments, New Castle, DE) at a heating rate of 10°C/min in air. Resonance Raman spectra were measured on an inVia H30434 Raman spectrophotometer (Renishaw, England). Electrochemical measurements were performed on a model CHI630D electrochemical analyzer (ChenHua Instruments Co. Ltd., Shanghai, China). All experiments were conducted using a three-electrode electrochemical cell consisting of a glassy carbon working electrode, a Ag/AgCl reference electrode and a platinum wire counter electrode.
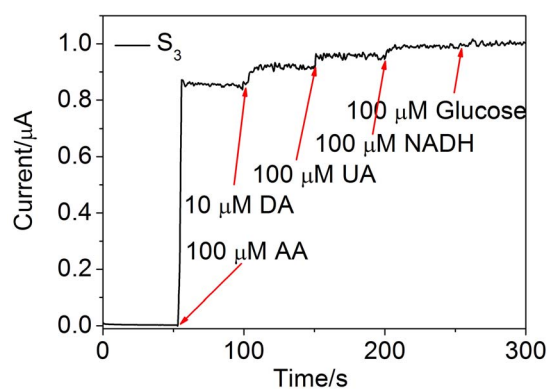

Figure 5 | Amperometric response of S3 at +0.15 V with successive additions of different analytes.

1. Agius, F. et al. Engineering increased vitamin C levels in plants by overexpression of a D-galacturonic acid reductase. Nat. Biotechnol. **21**, 177–181 (2003).
2. Green, M. & Fry, S. Vitamin C degradation in plant cells via enzymatic hydrolysis of 4-O-oxalyl-L-threonate. Nature **433**, 83–87 (2005).
3. Padayatty, S. J. et al. Vitamin C as an antioxidant: Evaluation of its role in disease prevention. J. Am. Coll. Nutr. **22**, 18–35 (2003).
4. Yang, J. J., Wu, J. Z. & Qiao, C. H. Expedient Synthesis of Epigoitrin from L-Ascorbic Acid. Synthetic Commun. **44**, 1240–1244 (2014).
5. Bautista-Ortega, J., Cortes-Cuevas, A., Ellis, E. A. & Ruiz-Feria, C. A. Supplemental (L)-arginine and vitamins E and C preserve xanthine oxidase activity in the lung of broiler chickens grown under hypobaric hypoxia. Poultry Sci. **93**, 979–988 (2014).
6. Sun, C. L., Lee, H. H., Yang, J. M. & Wu, C. C. The simultaneous electrochemical detection of ascorbic acid, dopamine, and uric acid using graphene/size-selected Pt nanocomposites. Biosens. Bioelectron. **26**, 3450–3455 (2011).
7. Ma, Y. et al. 3D graphene foams decorated by CuO nanoflowers for ultrasensitive ascorbic acid detection. Biosens. Bioelectron. **59**, 384–388 (2014).
8. Ammam, M. Electrochemical and electrophoretic deposition of enzymes: Principles, differences and application in miniaturized biosensor and biofuel cell electrodes. Biosens. Bioelectron. **58**, 121–131 (2014).
9. Wang, X. et al. Direct, reagentless electrochemical detection of the BIR3 domain of X-linked inhibitor of apoptosis protein using a peptide-based conducting polymer sensor. Biosens. Bioelectron. **61**, 57–62 (2014).
10. Kim, S. J. et al. Electrospun iridium oxide nanofibers for direct selective electrochemical detection of ascorbic acid. Sens. Actuat. B-Chem. **196**, 480–488 (2014).
11. Sun, C. L. et al. Microwave-Assisted Synthesis of a Core-Shell MWCNT/GONR Heterostructure for the Electrochemical Detection of Ascorbic Acid, Dopamine, and Uric Acid. Acs Nano **5**, 7788–7795 (2011).
12. Zhuang, Z. B., Sheng, W. C. & Yan, Y. S. Synthesis of Monodispere Au@Co3O4 Core-Shell Nanocrystals and Their Enhanced Catalytic Activity for Oxygen Evolution Reaction. Adv. Mater. **26**, 3950–3955 (2014).
13. Shearer, C. J., Cherevan, A. & Eder, D. Application and Future Challenges of Functional Nanocarbon Hybrids. Adv. Mater. **26**, 2295–2318 (2014).
14. Zhang, H. et al. Fabrication of nanoflower-like dendritic Au and polyaniline composite nanosheets at gas/liquid interface for electrocatalytic oxidation and sensing of ascorbic acid. Electrochem. Commun. **30**, 46–50 (2013).
15. Novoselov, K. S. et al. Electric field effect in atomically thin carbon films. Science **306**, 666–669 (2004).
16. Mohanty, N. & Berry, V. Graphene-Based Single-Bacterium Resolution Biodevice and DNA Transistor: Interfacing Graphene Derivatives with Nanoscale and Microscale Biocomponents. Nano Lett. **8**, 4469–4476 (2008).
17. Henriksen, E. A. et al. Cyclotron resonance in bilayer graphene. Phys. Rev. Lett. **100**, 087403 (2008).
18. Zhu, Y. W. et al. Carbon-Based Supercapacitors Produced by Activation of Graphene. Science **332**, 1537–1541 (2011).
19. Zope, B. N., Hibbit, D. D., Neurock, M. & Davis, R. J. Reactivity of the Gold/Water Interface During Selective Oxidation Catalysis. Science **330**, 74–78 (2010).
20. Yan, Y. M. et al. Biocatalytic growth of Au nanoparticles immobilized on glucose oxidase enhances the ferrocene-mediated bioelectrocatalytic oxidation of glucose. Adv. Mater. **20**, 2365–2370 (2008).
21. Cecchini, M. P. et al. Self-assembled nanoparticle arrays for multiphase trace analyte detection. Nat. Mater. **12**, 165–171 (2013).
22. Tian, X. et al. Simultaneous determination of L-ascorbic acid, dopamine and uric acid with gold nanoparticles-beta-cyclodextrin-graphene-modified electrode by square wave voltammetry. Talanta **93**, 79–85 (2012).
23. Goncalves, G. et al. Surface Modification of Graphene Nanosheets with Gold Nanoparticles: The Role of Oxygen Moieties at Graphene Surface on Gold Nucleation and Growth. Chem. Mater. **21**, 4796–4802 (2009).
24. Tesler Alexander, B. et al. Solid-State Thermal Dewetting of Just-Percolated Gold Films Evaporated on Glass: Development of the Morphology and Optical Properties. J. Phys. Chem. C **117**, 11337–11346 (2013).
25. Zhao, Y., Song, X., Song, Q. & Yin, Z. A facile route to the synthesis copper oxide/reduced graphene oxide nanocomposites and electrochemical detection of catechol organic pollutant. CrystEngComm. **14**, 6710–6719 (2012).

26. Zhou, M., Zhai, Y. & Dong, S. Electrochemical Sensing and Biosensing Platform Based on Chemically Reduced Graphene Oxide. *Anal. Chem.* **81**, 5603–5613 (2009).

27. Chen, H. *et al.* Mechanically strong, electrically conductive, and biocompatible graphene paper. *Adv. Mater.* **20**, 3557–3561 (2008).

28. Shang, N. G. *et al.* Catalyst-Free Efficient Growth, Orientation and Biosensing Properties of Multilayer Graphene Nanoflake Films with Sharp Edge Planes. *Adv. Funct. Mater.* **18**, 3506–3514 (2008).

29. Hu, G., Ma, Y., Guo, Y. & Shao, S. Electrocatalytic oxidation and simultaneous determination of uric acid and ascorbic acid on the gold nanoparticles-modified glassy carbon electrode. *Electrochim. Acta* **53**, 6610–6615 (2008).

30. Dong, X. C. *et al.* 3D Graphene-Cobalt Oxide Electrode for High-Performance Supercapacitor and Enzymeless Glucose Detection. *ACS Nano* **6**, 3206–3213 (2012).

31. Zhang, X., Lai, G., Yu, A. & Zhang, H. A glassy carbon electrode modified with a polyaniline doped with silicotungstic acid and carbon nanotubes for the sensitive amperometric determination of ascorbic acid. *Microchim. Acta* **180**, 437–443 (2013).

32. Abdelwahab, A. A., Kim, D., Halappa, N. & Shim, Y. A Selective Catalytic Oxidation of Ascorbic Acid at the Aminopyrimidyl Functionalized-Conductive Polymer Electrode. *Electroanal.* **25**, 1178–1184 (2013).

33. Weng, C. J. *et al.* Synthesis of electroactive mesoporous gold-organosilica nanocomposite materials via a sol-gel process with non-surfactant templates and the electroanalysis of ascorbic acid. *J. Mater. Chem. B* **1**, 4983–4991 (2013).

34. Mo, J. W. & Ogorevc, B. Simultaneous measurement at dopamine and ascorbate at their physiological levels using voltammetric microprobe based on overoxidized poly(1,2-phenylenediamine)-coated carbon fiber. *Anal. Chem.* **73**, 1196–1202 (2001).

35. Park, S., Chun, T. & Kim, H. Nonenzymatic glucose detection using mesoporous platinum. *Anal. Chem.* **75**, 3046–3049 (2003).

36. Yamada, K. *et al.* The simultaneous measurement of nicotinamide adenine dinucleotide and related compounds by liquid chromatography/electrospray ionization tandem mass spectrometry. *Anal. Biochem.* **352**, 282–285 (2006).

37. Cirillo, P. *et al.* Uric acid, the metabolic syndrome, and renal disease. *J. Am. Soc. Nephrol.* **17**, S165–8 (2006).

Acknowledgments

Author contributions

J.S. conducted the most of investigation for the samples and wrote the main paper. L.X. supervised the project, had given valuable advices on the proceeding of this work, and revised the manuscript. D.L.L. and H.W.S. had provided precious suggestions on the selection of test. R.Q.X., Q.L.L. and C.Y.Z. supported the characterization of the samples. All authors discussed the results and commented on the manuscript at all stages.

Additional information

Supplementary information accompanies this paper at http://www.nature.com/scientificreports

Competing financial interests: The authors declare no competing financial interests.

How to cite this article: Song, J. *et al.* Synthesis of Au/Graphene Oxide Composites for Selective and Sensitive Electrochemical Detection of Ascorbic Acid. *Sci. Rep.* **4**, 7515; DOI:10.1038/srep07515 (2014).